Echo motion imaging with adaptive clutter filter for assessment of cardiac blood flow

2015 Jpn. J. Appl. Phys. 54 07HF09

(http://iopscience.iop.org/1347-4065/54/7S1/07HF09)

Japanese Journal of Applied Physics **54**, 07HF09 (2015) **REGULAR PAPER**
http://dx.doi.org/**10.7567/JJAP.54.07HF09**

Echo motion imaging with adaptive clutter filter for assessment of cardiac blood flow

Hiroki Takahashi[1]*, Hideyuki Hasegawa[1,2], and Hiroshi Kanai[2,1]

[1]*Graduate School of Biomedical Engineering, Tohoku University, Sendai 980-8579, Japan*
[2]*Graduate School of Engineering, Tohoku University, Sendai 980-8579, Japan*
E-mail: h.takahashi@ecei.tohoku.ac.jp

Received December 10, 2014; accepted March 24, 2015; published online June 18, 2015

Visualization of the vortex blood flow in the cardiac chamber is a potential diagnostic tool for the evaluation of cardiac function. In the present study, a method for automatic selection of the desirable cutoff frequency of a moving target indicator filter, namely, a clutter filter, was proposed in order to visualize complex blood flows by the ultrahigh-frame-rate imaging of echoes from blood particles while suppressing clutter echoes. In this method, the cutoff frequency was adaptively changed as a function of the velocity of the heart wall (clutter source) in each frame. The feasibility of the proposed method was examined through the measurement of a healthy volunteer using parallel receive beamforming with a single transmission of a non-steered diverging beam. Using the moving target indicator filter as above with the cutoff frequency determined by the proposed method, the vortex-like blood flow in the cardiac chamber was visualized as movements of echoes from blood particles at a very high frame rate of 6024 Hz while suppressing clutter echoes.

1. Introduction

In recent years, the understanding of the behavior of the blood flow in the cardiac chamber has progressed because the method for imaging the cardiac flow has been increasingly improved, for instance, color Doppler flow imaging, echocardiographic particle image velocimetry (E-PIV), and phase-contrast magnetic resonance imaging (PC-MRI). In particular, the role of the vortex-like blood flow in the cardiac chamber has been strongly focused on. It is assumed that vortices contribute to blood smoothly flowing out to the aorta by preserving the momentum of blood in the diastolic phase.[1)] Such flow behavior would enhance the cardiac pumping efficiency owing to the ejection of blood in the chamber with a smaller energy provided by the myocardium. Hence, visualization of the vortex blood flow would be a new diagnostic tool for the evaluation of cardiac function. However, a PC-MRI scanner is expensive and unsuitable for screening tests due to the long time required for scanning. On the other hand, echocardiography provides cross-sectional images noninvasively in real time; therefore, it is useful valuable if a complex blood flow such as the vortex flow can be easily visualized using echocardiography. In medical ultrasound, the color Doppler method is a major diagnostic implement for visualizing the cardiac blood flow. The true direction of the blood flow, however, cannot be shown because the Doppler measurement only reveals the axial velocity.

Various techniques have been developed and studied to reveal the direction of blood flows.[2)] A technique with two crossed transmit/receive beams utilizing the Doppler spectral broadening effect has been proposed to estimate the transverse velocity component (perpendicular to the ultrasonic beam) at a specific point.[3,4)] The velocity vector of the blood flow was estimated by combining Doppler measurement from two (or more) directions.[5,6)] Recently, the imaging of blood velocity vectors estimated by the vector Doppler technique with transmissions of crossed plane waves has been achieved.[7,8)] A method for imaging blood velocity vectors using multiple transmissions of steered plane waves and a least squares fitting with velocities in different directions was also developed.[9)] These techniques, however, require a relatively large beam steering angle and, thus, their application is limited to blood flows in a shallow region, such like the carotid blood flow. Hence, the vector Doppler technique is not suitable for normal cardiac measurement with a phased-array transducer. As a result, a linear-array transducer with a large aperture is used in ongoing studies.

A method for estimation of the direction of a blood flow was developed that traces the interframe movement of echoes between successive frames by searching for the maximal correlation between echoes in the kernels in successive frames (called the speckle tracking technique).[10)] The speckle tracking technique has been also used for estimation of myocardial velocity.[11)] Løvstakken et al. proposed a method for contrast-free imaging of the blood flow direction from the movements of echoes from blood particles obtained by the customized sweeping of a focused beam.[12)] This method, however, has the critical issue of an insufficient frame rate because multiple transmissions in the same direction are needed for visualization of the echoes from blood particles. As a result, the two-dimensional (2D) blood velocity vectors could not be estimated by the speckle tracking technique due to the low continuity of the movement of echoes between consecutive frames as described in Ref. 12. Recently, the imaging of 2D blood velocity vectors estimated by the speckle tracking technique with high-frame-rate measurement by plane wave transmission and parallel receive beamforming has been shown to be feasible.[13)] More recently, the imaging of 2D blood velocity vectors estimated in the frequency domain by plane wave imaging was also demonstrated.[14)] The application of fast ultrasound imaging with parallel beamforming has been broadened to the monitoring of areas treated by ultrasonic therapy.[15)] The width of the region illuminated by a plane wave is limited by the aperture size of the transducer. In echocardiography, a phased-array transducer with a small aperture is used because the heart must be insonified from a narrow acoustic window between ribs. This means that the use of the transmission of the plane wave requires many transmissions per frame and limits the frame rate in echocardiography. Plane wave imaging, therefore, would be not suitable for visualizations of the cardiac blood flow requiring a high-frame-rate measurement.

As a different approach to estimating the transverse component in the blood flow velocity, vector flow mapping has been developed.[16)] In vector flow mapping, the transverse

flow velocity is mathematically calculated from the 2D distribution of the axial velocity measured by the color Doppler method on the basis of the hydrokinetic assumption. In another method, the velocity of the surrounding heart wall estimated by the speckle tracking method has been utilized to obtain a more accurate boundary condition in the continuity equation.[17,18] Although these calculation techniques can depict the intraventricular flow behavior, the radical flow of blood cannot be visualized.

In our previous study, it was shown that the direction of the blood flow in the cardiac lumen could be visualized by the very high frame rate (kHz order) measurement of echoes from blood particles using parallel beamforming coupled with transmissions of diverging waves.[19] High-pass filtering in the direction of the frame [called the moving target indicator (MTI) filtering] has been used to suppress the undesirable echoes from ribs and the heart wall. The cutoff frequency for the MTI filter was set to match the typical maximal velocity of the heart wall and was fixed throughout the cardiac cycle. However, the velocity of the heart wall changes over time during the entire cardiac cycle; therefore, the cutoff frequency should fluctuate depending on the heart wall velocity to increase the detectivity of echoes from blood particles in a slow flow.

In the present study, a method for automatic selection of the cutoff frequency in MTI filtering was proposed. In this method, the cutoff frequency of the MTI filter was adaptively changed depending on the velocity of the heart wall in each frame. The feasibility of the proposed method was examined by comparison between blood echo images obtained by MTI filtering with static and automatically selected cutoff frequencies through an in vivo experiment. In the first part of this paper, a strategy for the ultrahigh-frame-rate imaging of movements of echoes from blood particles is described in Sect. 2.1. The ultrahigh-frame-rate imaging was implemented using parallel receive beamforming with the transmission of a single diverging beam. In Sect. 2.1, a procedure to suppress sidelobe levels in echoes from blood particles using the phase coherence factor with sub-beamformers (PCF-SB)[20] is also presented. In Sect. 2.2, the proposed adaptive MTI filtering is presented. Our in vivo experimental result used to examine the feasibility of the proposed MTI filtering is reported in Sect. 3 and discussed in Sect. 4.

2. Principles

2.1 Ultrahigh-frame-rate echocardiography with improved image quality

A modified diagnostic ultrasound system (Hitachi-Aloka Medical Alpha10) with a commercial 3.75 MHz phased array transducer was used to acquire ultrasonic RF echo signals from 96 transducer elements. RF signals received by individual elements were sampled at 15 MHz for off-line processing by a personal computer. Using individual RF signals obtained by the transmission of a single diverging wave, high-frame-rate echocardiography was realized by parallel receive beamforming.[21–23] The acquisition frame rate decreases with increasing number of transmissions per frame. A strategy for the high-frame-rate imaging of echoes from blood particles is described in this section.

In high-frame-rate echocardiography, the lateral spatial resolution and the sidelobe characteristics can be improved by compounding (averaging) the echo signals acquired by transmissions at different steering angles. Although the image quality is improved by this compounding technique, a higher frame rate, i.e., fewer transmissions, is desirable for visualization of the cardiac blood flow in order to avoid the signal decorrelation caused by the fast (maximal velocity of over 1 m/s) and complex blood flow in the cardiac lumen.

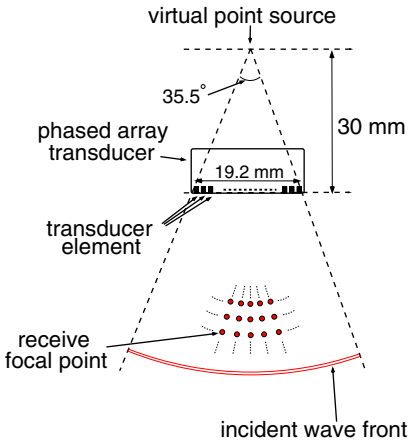

Fig. 1. (Color online) Illustration of transmission of spherically diverging beam and parallel receive beams.

The frame rate required for visualization of the cardiac blood flow was examined through a steady-flow experiment. Echoes from a blood-mimicking fluid (BMF) steadily flowing in a cylindrical flow path (diameter of 8 mm) surrounded by tissue-mimicking rubber were measured. The angle between the transducer surface and the flow axis was set at 56°. The transducer surface was placed at a distance of 7 cm from the outer surface of the flow path. The flow rate, which corresponds to the mean flow velocity, was measured by a mass flow meter connected to the flow path. The echo data were acquired at a frame rate of 6024 Hz by the single transmission of a non-steered diverging beam per frame at a flow rate of 0.6 L/min (mean flow velocity: 0.2 m/s, Reynolds number: 960). An illustration of the beamforming is shown in Fig. 1. The transmit wave diverged from a virtual point source placed 30 mm behind the array surface. In this measurement, the accuracy of velocity estimation was evaluated for different frame rates at a constant Reynolds number of 960. RF echo signals for different frame rates (1506, 2008, 3012, and 6024 Hz) were simulated by changing the frame interval of the acquired echo data. A higher flow rate of 1.8 L/min (mean flow velocity of 0.6 m/s) was also simulated for each set of echo data with further changes in the frame interval. Figure 2 shows the mean flow velocities obtained from the velocity vectors estimated by the speckle tracking technique with the temporal averaging of 2D correlation functions. On the assumption that the distribution of the flow velocity follows the Hagen–Poiseuille equation,[24] the mean flow velocity was computed as follows:

$$\bar{V} = \frac{1}{A}\sum_{j=0}^{N_j-1}(\pi r_j \Delta r)\mathbf{v}_j \cdot \mathbf{n}, \tag{1}$$

where $\mathbf{v}_j$, r_j, Δr, A, and $\mathbf{n}$ are the velocity vector estimated at the jth spatial point, the distance from the center of the flow path to the jth spatial point, the interval between the jth and $(j+1)$th spatial points, the cross-sectional area of the flow

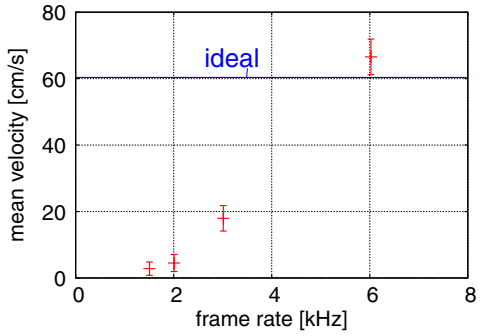

Fig. 2. (Color online) Mean flow velocities estimated at different frame rates in steady-flow measurements. The standard deviations were computed from 50 frames.

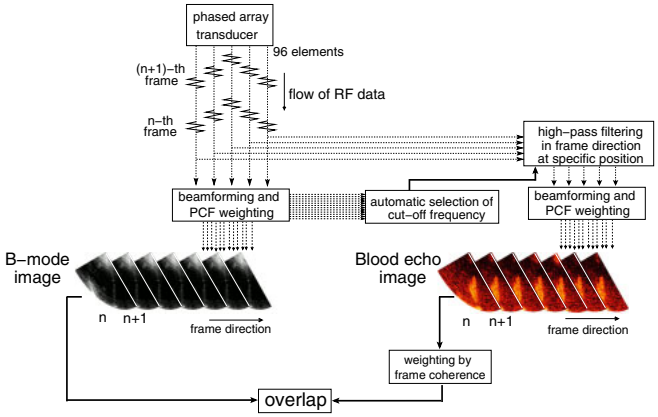

Fig. 3. (Color online) Schematic of proposed sequence of procedures for imaging of echoes from blood particles.

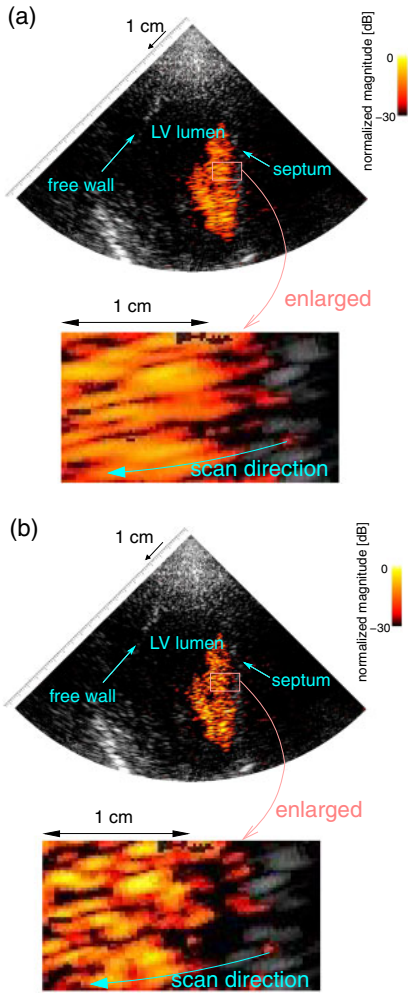

Fig. 4. (Color online) Enlarged blood echo images in in vivo experiment on a healthy volunteer (a) without weighting and (b) with weighting by the PCF-SB. In the blood echo image, the intensity of MTI-filtered echo signals was color-coded according to a hot scale.

path, and the unit vector parallel to the flow direction, respectively. The interval between the jth and $(j+1)$th spatial points was set at 0.4 mm. As shown in Fig. 2, it was found that a high frame rate of 6 kHz was required to measure the fast blood flow. Therefore, the ultrahigh-frame-rate measurement was performed with the single transmission of the diverging beam per frame.

The contrast of the B-mode and blood echo images was low due to high sidelobe levels caused by the transmission of unfocused ultrasound. To improve the image quality without decreasing the frame rate, we employed special beamforming with the PCF-SB. This technique improves the sidelobe characteristics and the spatial resolution by utilizing the diversity of echo signals received by transducer elements. Through phantom and in vivo experiments, the strategy of the PCF-SB was shown to be effective for improving the quality of B-mode images.[20] It has also been found that the improvement of the sidelobe characteristics in blood echo imaging using the PCF-SB is feasible.[25]

The proposed sequence of procedures is shown in Fig. 3. B-mode images were created using beamformed RF signals weighted by the PCF-SB. On the other hand, MTI filtering was applied to individual echo signals received by transducer elements. Then, the PCF-SB for the blood echo image was computed from the filtered element signals. As with B-mode imaging, beamformed signals after the MTI filtering were weighted using the PCF-SB. In our study, the brightness in a blood echo image corresponds to the intensity of MTI-filtered echo signals. Figure 4 shows blood echo images (hot-scaled) without weighting and with weighting by the PCF-SB for blood echo imaging with B-mode images (gray-scaled). As shown in Fig. 4, speckle echoes from blood particles became sharper as a result of improving the sidelobe characteristics of MTI-filtered echoes. Toward the imaging of blood echoes with a high contrast, beamformed RF signals obtained with the PCF-SB were further weighted by the coherence in time (frame) variation.[19] We defined this frame coherence as the temporal-averaged power of the complex correlation of demodulated signals between successive frames at a lag of zero normalized by the power of the signals. The frame coherence decreases with the variation of the temporal change in the phase of echoes. MTI-filtered and beamformed echo signals in six neighboring frames were used for computation of the frame coherence.

2.2 Adaptive selection of cutoff frequency in MTI filtering

The amplitude of echoes from the ribs and heart wall is much larger than that from blood particles. Therefore, echoes from blood particles in the direction of the main lobe are contaminated even by sidelobe echoes from clutter sources such as the ribs and the heart wall. The maximal velocity of the heart wall is almost 10 cm/s, while that of the cardiac blood flow reaches over 1 m/s. Hence, clutter echoes from

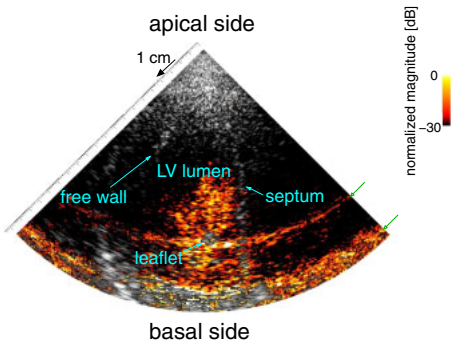

Fig. 5. (Color online) Sidelobe artifact captured in early diastole in in vivo experiment on a healthy volunteer. The green arrows indicate the sidelobe artifacts. The cutoff frequency of the MTI filter was set at 650 Hz.

the ribs and heart wall are suppressed by MTI filtering, which corresponds to applying high-pass filtering to echoes from a specific position in the direction of the frame.

Regarding the blood echo image obtained with unfocused transmission, a serious artifact is generated by sidelobe echoes from clutter sources due to the high sidelobe level when the cutoff frequency of the MTI filter is lower than the desirable value. Figure 5 shows the blood echo image (hot-scaled) with the B-mode image (gray-scaled) in early diastole. The green arrows indicate beltlike artifacts originating from sidelobes. As shown in Fig. 5, the artifacts interfere with echoes from blood particles in the cardiac lumen. The levels of clutter echoes are intensified at a low cutoff frequency of the MTI filter. On the other hand, the detectability of a slow blood flow is degraded when the cutoff frequency of the MTI filter is high.

The velocity of the heart wall changes over time. Therefore, the cutoff frequency of the MTI filter desirable for the detection of a slow blood flow depends on the cardiac phase. In the present study, the cutoff frequency of the MTI filter was adaptively changed over time as a function of the velocity of the heart wall. First, echo signals from the ribs and heart wall (clutter sources) were identified (labeled) on the basis of the amplitude of the RF signal using the *k*-means clustering technique.[26] In this technique, the means of features belonging to different groups are updated repeatedly while all points are discerned so that the distance between the mean feature of each group and the feature of each point is small. Then, in regard to the echo signals from the clutter sources, the mean frequency μ of the echo signal in the direction of the frame and the standard deviation σ were estimated by the autocorrelation technique.[27] Because the velocity of the heart wall fluctuates spatially and temporally, the deviation of the frequency of echoes in the direction of the frame should be considered in the determination of the cutoff frequency. We defined the cutoff frequency as $f_{\mathrm{cut}} = \mu + n\sigma$, where n is an integer.

For evaluation of the difference in the myocardial velocities between different spatial positions, the spatial average μ_{f}^{Π} and its standard deviation $\sigma_{\mathrm{f}}^{\Pi}$ were estimated using f_{cut} in each position labeled as the heart wall, and the cutoff frequency in the frame was set to $f_{\mathrm{cut.sp}} = \mu_{\mathrm{f}}^{\Pi} + 3\sigma_{\mathrm{f}}^{\Pi}$. Note that echo signals with a very slow variation in the direction of the frame were omitted in the following analysis. The ribcage is almost static in the entire cardiac cycle;

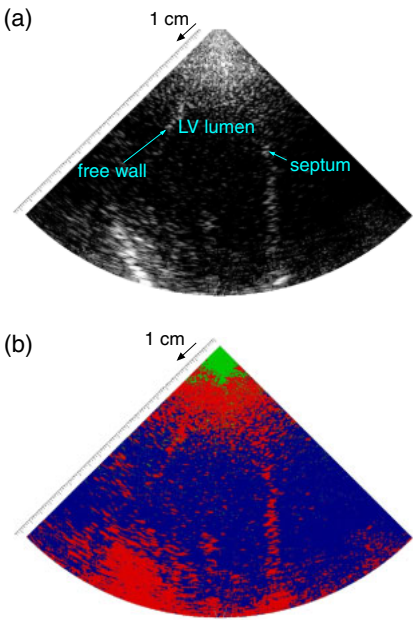

Fig. 6. (Color online) (a) B-mode image and (b) distribution of points labeled as the heart wall (red) and ribs (green) by *k*-means clustering.

therefore, the cutoff frequency can be underestimated if echoes from ribs are used in the calculation of μ_{f}^{Π} and $\sigma_{\mathrm{f}}^{\Pi}$. μ_{f}^{Π} and μ_{f}^{Π} were computed excluding echoes from tissues with a velocity below 0.2 mm/s, which were assumed to be echoes from ribs. Figures 6(a) and 6(b) respectively show the B-mode image and points labeled as the heart wall (red) and ribs (green) by *k*-means clustering. The cutoff frequencies $f_{\mathrm{cut.sp}}$ were temporally averaged in the direction of the frame to prevent a large variation of the cutoff frequency in near by frames. The impulse response of the MTI filter was generated by a 60th-order sinc function multiplied by the Kaiser window function, and the cutoff frequency was automatically determined in each frame.

3. In vivo experimental result for a human heart

RF echo signals from the left ventricle were measured at a frame rate of 6024 Hz in a transthoracic three-chamber view of a 27-year-old healthy volunteer. Figure 7 shows the cutoff frequency automatically determined at $n = 3$. Figure 8 shows blood echo images obtained at $n = 1$, 2, and 3 in the frame indicated by the blue dashed line in Fig. 7 (when the cutoff frequency was minimum in diastole). In Fig. 8, the B-mode images were not superimposed. Echoes from the heart wall significantly contaminated those from blood particles at $n = 1$ in Fig. 8(a), and echoes from the free wall surrounded by the cyan dashed line remained at $n = 2$ in Fig. 8(b). Therefore, the cutoff frequency was defined as $f_{\mathrm{cut}} = \mu + 3\sigma$.

Figure 9(1) shows the blood echo images with the B-mode images in the frame in early diastole, which was indicated as (1) in Fig. 7. In Figs. 9(a-1), 9(b-1), and 9(c-1), blood echo images were obtained using MTI filters with different cutoff frequencies of 300 and 650, which were constant in the entire cardiac cycle, and 1059 Hz, which was determined by the proposed method, respectively. Figure 9(2) shows the blood echo images with the B-mode images obtained in the frame in mid diastole, which was indicated as (2) in Fig. 7, at different cutoff frequencies of 300, 650, and 410 Hz (the proposed method).

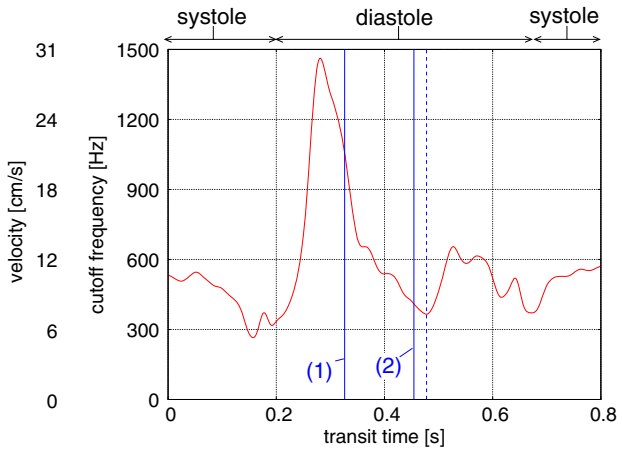

Fig. 7. (Color online) Automatically determined cutoff frequencies in entire cardiac cycle. The blue dashed line and blue solid lines indicate the time at which the blood echo images shown in Fig. 8 and Figs. 9(1), and 9(2) were obtained, respectively.

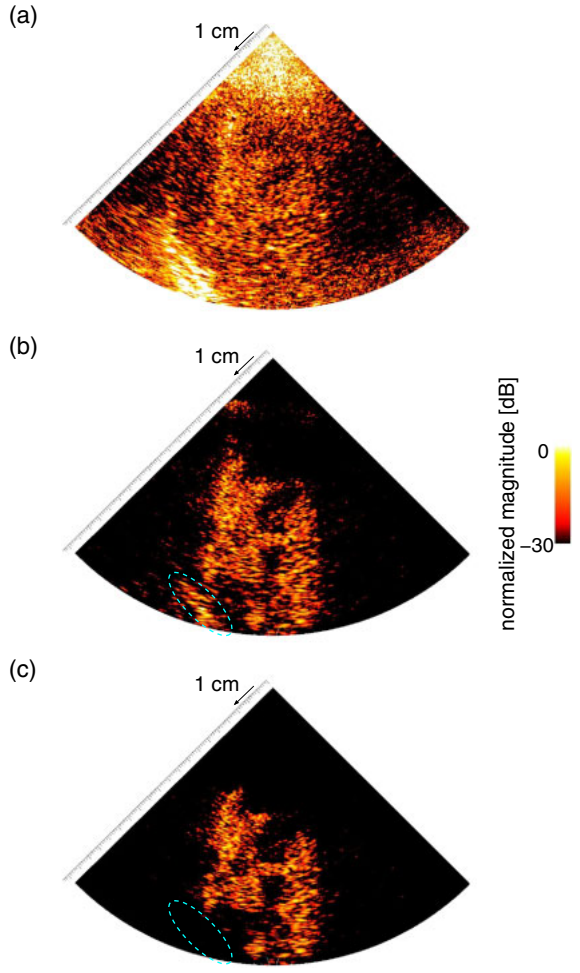

Fig. 8. (Color online) Blood echo images obtained by determining the cutoff frequency f_{cut} as (a) $f_{cut} = \mu + \sigma$, (b) $\mu + 2\sigma$, and (c) $\mu + 3\sigma$ in the frame indicated by the blue dashed line in Fig. 7.

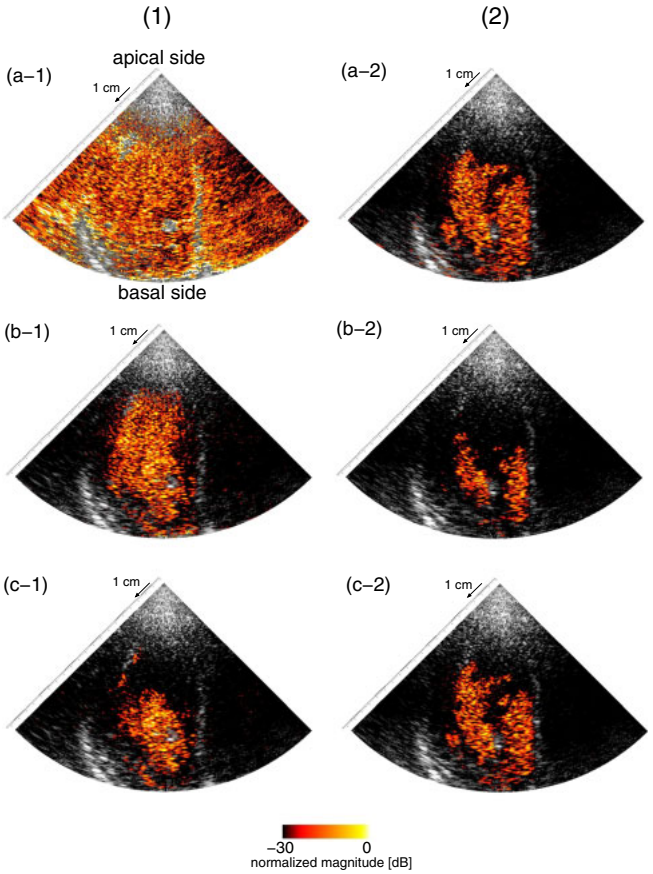

Fig. 9. (Color online) Blood echo images obtained from frames in (1) early diastole and (2) mid-diastole (a) by MTI filtering with a cutoff frequency of 300 Hz, (b) by MTI filtering with a cutoff frequency of 650 Hz, and (c) by MTI filtering with cutoff frequencies of 1059 Hz in (1) and 410 Hz in (2) determined by our proposed method.

As shown in Figs. 9(a-1) and 9(a-2), echoes from blood particles are visualized in a wider region in mid-diastole using the low cutoff frequency of 300 Hz, but more clutter echoes are seen in early diastole. Using the MTI filter with the cutoff frequency of 650 Hz, echoes from blood particles flowing into the cardiac lumen are visible with suppressed clutter echoes in early diastole as shown in Fig. 9(b-1). However, as shown in Fig. 9(b-2), the echoes from blood particles have lower intensities than those in Fig. 9(a-2). As shown in Fig. 9(c-2) obtained by our proposed method, although visible echoes from blood particles are slightly less intense than those in Fig. 9(a-2), echoes from blood particles in the vortex flow can be seen over a wider field in mid-diastole, while clutter echoes are sufficiently suppressed in early diastole.

Figure 10 shows 2D velocity vectors of the blood flow estimated by the speckle tracking technique[10] at cutoff frequencies of 650, 300, and 410 Hz (the proposed method) in the same frame as in Fig. 9. The spatial points at which 2D velocity vectors were estimated were manually assigned at a regular interval inside the cardiac lumen. Vector magnitudes at all pixels were obtained by reconstructive interpolation[28] of the distribution of the 2D vector velocity. The size of the spatial window for the computation of the 2D correlation function in the speckle tracking technique was set to 9° and 8.2 mm in the lateral and axial directions, respectively. 2D correlation functions were temporally averaged over 12 frames corresponding to almost 2 ms.[29] The averaged 2D correlation function was up-sampled by reconstructive interpolation[28] in order to measure the small movement of echoes between successive frames. In Fig. 10(a), a discontinuous distribution of velocity vectors can be observed in the green circle due to the low detectivity of echoes from blood

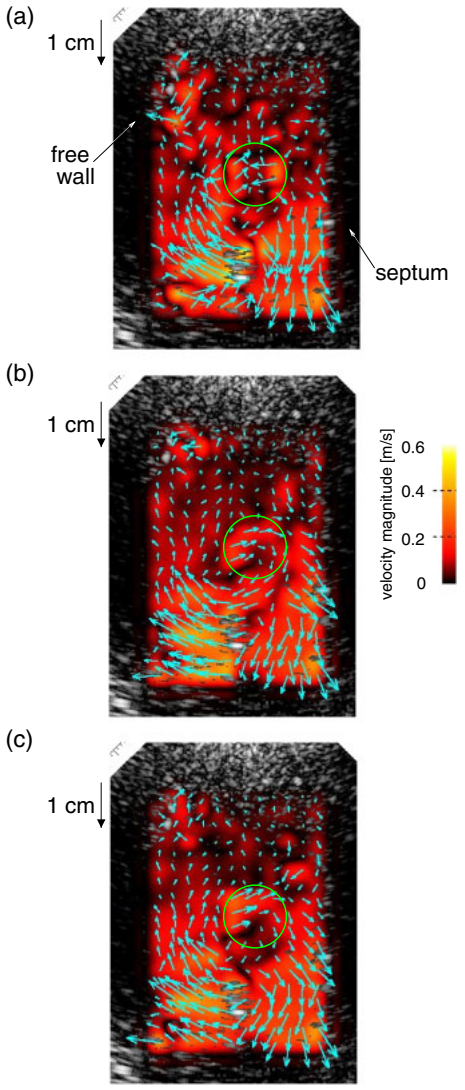

Fig. 10. (Color online) 2D velocity vectors of blood flow estimated by the speckle tracking technique with temporally averaged 2D correlation function at fixed cutoff frequencies of (a) 650 Hz and (b) 300 Hz and at the cutoff frequency of (c) 410 Hz determined by our proposed method in mid-diastole. The cyan arrows and the hot color-coded intensity indicate the direction and magnitude of the 2D velocity vectors, respectively.

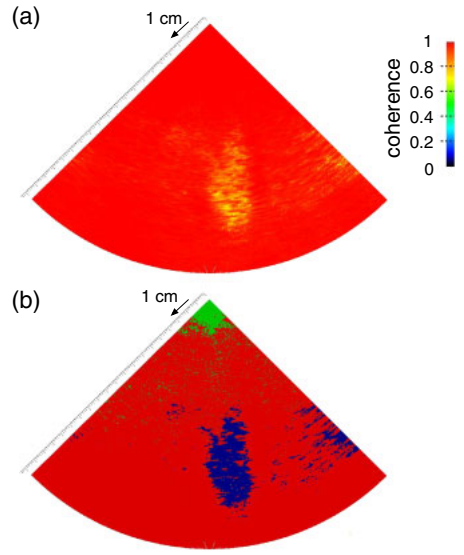

Fig. 11. (Color online) (a) Distribution of coherence in direction of frame and (b) distribution of points labeled as the heart wall (red) and ribs (green) by *k*-means clustering in the same frame as in Fig. 6. The coherence was coded according to the right color bar.

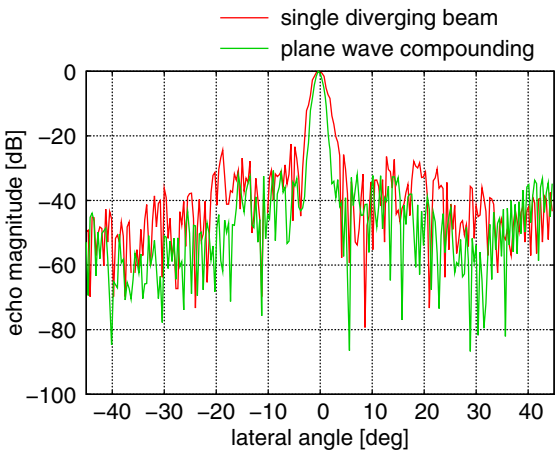

Fig. 12. (Color online) Lateral profiles of amplitude of an echo from a wire placed in water at a distance of 7 cm. Amplitude profiles were obtained (a) by no compounding with the single diverging transmission and (b) by compounding with transmissions of the plane wave in seven directions.

particles in the slow flow. The peak values of the 2D correlation functions averaged for all velocity vectors were 0.77 in Fig. 10(a), 0.86 in Fig. 10(b), and 0.85 in Fig. 10(c). In Fig. 10(c), the rotation of the flux in the clockwise direction was revealed by the distribution of the 2D velocity vectors. The proposed adaptive MTI filtering was effective for improving the accuracy of velocity vector estimation by enhancing the detectivity of echoes from blood particles.

4. Discussion

To determine the cutoff frequency of the MTI filter, only the amplitude of echoes was used for the identification of echoes from the heart wall by the *k*-means clustering method. An alternative method for the identification of echoes from the heart wall using the coherence in the direction of the frame has also been proposed by our group.[30,31] Figures 11(a) and 11(b) show the distribution of the frame coherence and the region identified as the heart wall by the *k*-means clustering method using the frame coherence in the same frame as in Fig. 6. In contrast to Fig. 6(b), it can be seen that all the regions except for the septum and the free wall were misclassified as the heart wall in Fig. 11(b) because the coherence in such regions is high.

The reason for the high coherence in the cardiac lumen is considered to be that echoes from blood particles inside the cardiac lumen were contaminated by sidelobe echoes originating from the surrounding heart wall. In the previous studies of our group,[30,31] parallel receive beamforming with the transmission of plane waves in five or seven directions was performed, and the coherence in the direction of the frame at each spatial point was estimated using echo signals compounded in different transmissions. Figure 12 shows lateral profiles of the amplitude of an echo from a wire obtained by the single diverging beam transmission used in the present study and by compounding seven transmissions of the plane wave with an angular interval of 6°. The wire was placed in water at a distance of 7 cm from the transducer

surface. The ratios of the echo magnitude averaged in lateral angle θ ranges of $-45° < \theta < -4.5°$ and $4.5° < \theta < 45°$ to the peak magnitude were evaluated to be -38.8 dB for the transmission of the single diverging beam and -45.3 dB for the transmission of seven plane waves. Hence, the echoes originating from sidelobes in the case of the compounding of echoes obtained by plane wave transmissions in seven directions were smaller than those in the case of the single diverging beam transmission. The number of transmissions per frame should be one in order to prioritize increasing the frame rate for visualization of the fast cardiac blood flow. Under such conditions, the use of the frame coherence is considered to be unsuitable for identification of the heart wall in ultrahigh-frame-rate measurement.

Echoes from blood particles on the apical side were more clearly visualized in the blood echo image in Fig. 9(b-1) with a fixed cutoff frequency of 650 Hz than those in Fig. 9(c-1) obtained by our proposed method. This means that the blood flow on the apical side of the cardiac lumen was slow relative to the basal side, and echoes from such regions were suppressed by the MTI filtering with the determined cutoff frequency of 1059 Hz. In early diastole, the leaflets of the mitral valve, which are one of the clutter sources, independently move very rapidly due to the inertial force of the blood flowing into the left ventricular chamber. In the proposed method, the spatial variation of the mean frequency in the direction of the frame was used for determination of the desirable cutoff frequency. Therefore, in early diastole, it was considered that the determined cutoff frequency was higher than the desirable value due to the large diversity of velocities in the clutter sources.

A radical solution to this problem is to determine the cutoff frequency of the MTI filter at each location by expanding our proposed method. As shown in Fig. 5, in high-frame-rate echocardiography with diverging beam transmission, the artifact echoes originating from sidelobes are generated in the lateral direction along the wave front of the diverging beam across a clutter source. Here, the cutoff frequency of the MTI filter was overestimated due to the large diversity of velocities in the clutter sources. Hence, it may be effective to adaptively change the cutoff frequency of the MTI filter at each location according to the velocity of the clutter source such as the ribs, heart wall, and cardiac valve. To consider the feasibility of this method, the mean frequencies of echoes from the heart wall and the leaflet in the direction of the frame were obtained using echoes from the corresponding regions in the same frame as in Fig. 9(1). Echoes from the regions filled in red in Fig. 13(a) were used for evaluation of the mean frequencies. Using the autocorrelation technique, the mean frequencies μ of the regions on the apical side of the septum and the leaflet of the mitral valve were evaluated to be 230 and 409 Hz, respectively. Then, to evaluate the effect of adaptively changing the MTI filtering depending on the location, the cutoff frequency of the MTI filter over the whole region was determined as $f_{\mathrm{cut.sp}} = \mu + 3\sigma$ using the mean frequency μ and the standard deviation σ in the direction of the frame obtained with echoes from either the septum or the leaflet. Figures 13(b) and 13(c) show the blood echo images obtained by the cutoff frequencies of 665 and 548 Hz determined using echoes from the regions in the leaflet and the septum indicated in Fig. 13(a), respectively. The cyan lines indicate a region on the apical side of the left ventricular lumen. Echoes from blood particles in this apical region in Fig. 13(c) were stronger than those in Fig. 13(b). Therefore, adaptively changing the MTI filtering depending on the location would be effective to increase the detectivity of blood flows.

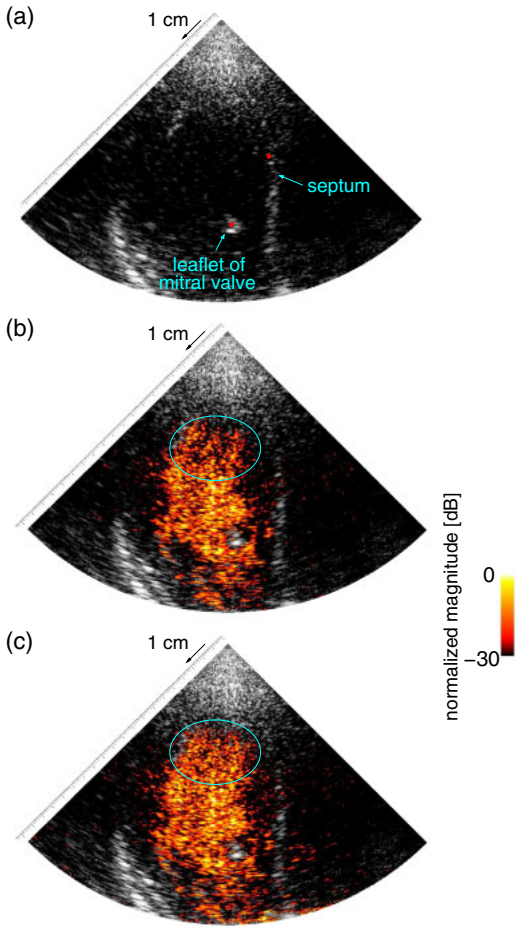

Fig. 13. (Color online) Regions assigned for evaluation of mean frequencies and for determination of cutoff frequencies. (a) Echoes in the regions in the septum and the leaflet filled in red were used. Blood echo images obtained by the cutoff frequencies determined using echoes from (b) the leaflet and (c) the septum.

5. Conclusions

A method for automatic selection of the cutoff frequency in the MTI filter has been proposed that increases the detectivity of echoes from a slow blood flow while suppressing clutter echoes. Ultrahigh-frame-rate measurement by parallel beamforming with the single transmission of a non-steered diverging beam was implemented to follow the fast blood flow in the cardiac lumen. The feasibility of the proposed method was examined in terms of the visibility of echoes from blood particles and the suppression of clutter echoes through an in vivo experiment on a 27-year-old volunteer. Although echoes from blood particles on the apical side were suppressed in early diastole, the detectivity of the blood flow was improved within the vortex-like blood flow of the cardiac lumen in mid diastole. Furthermore, it was confirmed that the proposed adaptive MTI filter was effective for increasing the accuracy of estimation of the blood velocity vector by the speckle tracking technique.

Acknowledgments

This work was supported by JSPS Research Fellowships for Young Scientists (DC1) and the International Advanced Research and Education Organization of Tohoku University.

1) P. P. Sengupta, G. Pedrizzetti, P. J. Kilner, A. Kheradvar, T. Ebbers, G. Tonti, A. G. Fraser, and J. Narula, J. Am. Coll. Cardiol. Imaging **5**, 305 (2012).
2) C. L. de Korte, M. M. Nillesen, A. E. C. M. Saris, R. G. P. Lopata, J. M. Thijssen, and L. Kapusta, J. Med. Ultrason. **41**, 279 (2014).
3) P. Tortoli, G. Guidi, and P. Pignoli, Ultrasound Med. Biol. **19**, 115 (1993).
4) P. Tortoli, A. Dallai, E. Boni, L. Francalanci, and S. Ricci, Ultrasound Med. Biol. **36**, 488 (2010).
5) M. D. Fox, IEEE Trans. Sonics Ultrason. **25**, 281 (1978).
6) L. Capineri, M. Scabia, and L. Masotti, Ultrasound Med. Biol. **28**, 237 (2002).
7) I. K. Ekroll, A. Swillens, P. Segars, T. Dahl, H. Torp, and L. Løvstakken, IEEE Trans. Ultrason. Ferroelectr. Freq. Control **60**, 727 (2013).
8) S. Ricci, L. Bassi, and P. Tortoli, IEEE Trans. Ultrason. Ferroelectr. Freq. Control **61**, 314 (2014).
9) B. Y. S. Yiu, S. S. M. Lai, and A. C. H. Yu, Ultrasound Med. Biol. **40**, 2295 (2014).
10) L. N. Bohs, B. J. Geiman, M. E. Anderson, S. C. Gebhart, and G. E. Trahey, Ultrasonics **38**, 369 (2000).
11) D. Asari, H. Hasegawa, and H. Kanai, Jpn. J. Appl. Phys. **53**, 07KF21 (2014).
12) L. Løvstakken, S. Bjærum, D. Martens, and H. Torp, IEEE Trans. Ultrason. Ferroelectr. Freq. Control **53**, 289 (2006).
13) J. Udesen, F. Gran, K. L. Hansen, J. A. Jensen, C. Thomsen, and M. B. Nielsen, IEEE Trans. Ultrason. Ferroelectr. Freq. Control **55**, 1729 (2008).
14) M. Lenge, A. Ramalli, E. Boni, H. Liebgott, C. Cachard, and P. Tortoli, IEEE Trans. Ultrason. Ferroelectr. Freq. Control **61**, 1504 (2014).
15) S. Sasaki, R. Takagi, K. Matsuura, S. Yoshizawa, and S. Umemura, Jpn. J. Appl. Phys. **53**, 07KF10 (2014).
16) S. Ohtsuki and M. Tanaka, J. Visualization **9**, 69 (2006).
17) D. Garcia, J. C. D. del Álamo, D. Tanné, R. Yotti, C. Cortina, E. Bertrand, J. C. Antoranz, E. Pérez-David, R. Rieu, F. Fernández-Avilés, and J. Bermejo, IEEE Trans. Med. Imaging **29**, 1701 (2010).
18) K. Itatani, T. Okada, T. Uejima, T. Tanaka, M. Ono, K. Miyaji, and K. Takenaka, Jpn. J. Appl. Phys. **52**, 07HF16 (2013).
19) H. Takahashi, H. Hasegawa, and H. Kanai, Jpn. J. Appl. Phys. **53**, 07KF08 (2014).
20) H. Hasegawa and H. Kanai, IEEE Trans. Ultrason. Ferroelectr. Freq. Control **61**, 1779 (2014).
21) H. Hasegawa and H. Kanai, J. Med. Ultrason. **38**, 129 (2011).
22) H. Hasegawa and H. Kanai, IEEE Trans. Ultrason. Ferroelectr. Freq. Control **59**, 2569 (2012).
23) H. Hasegawa and H. Kanai, Jpn. J. Appl. Phys. **53**, 07KF02 (2014).
24) M. Hino, *Ryūtai Rikigaku* (Fluid Mechanics) (Asakura, Tokyo, 1992) Chap. 8 [in Japanese].
25) H. Takahashi, H. Hasegawa, and H. Kanai, Proc. IEEE Ultrasonics Symp., 2014, p. 341.
26) C. M. Bishop, *Pattern Recognition and Machine Learning* (Springer, Berlin, 2006) Chap. 9.1.
27) C. Kasai, K. Namekawa, A. Koyano, and R. Omoto, IEEE Trans. Sonics Ultrason. **32**, 458 (1985).
28) I. Cespedes, Y. Huang, J. Ophir, and S. Sprat, Ultrason. Imaging **17**, 142 (1995).
29) H. Takahashi, H. Hasegawa, and H. Kanai, J. Med. Ultrason. (in press) [DOI: 10.1007/s10396-015-0620-x].
30) H. Takahashi, H. Hasegawa, and H. Kanai, Jpn. J. Appl. Phys. **52**, 07HF17 (2013).
31) K. Nakahara, H. Hasegawa, and H. Kanai, Jpn. J. Appl. Phys. **53**, 07KF09 (2014).